A Comparison of Discrete and Continuum Simulations of the Das Sarma-Tamborenea Growth Model

Ali Emre Özer

CID: 01415475

Supervisor: Professor Dimitri Vvedensky

Assessor: Dr. Derek Lee

Word count: 5285

Contents

0   Summary

Surface growth processes are a subset of non-equilibrium systems which exhibit self-organized criticality. Such systems naturally evolve to a state where fluctuations are self-similar and exhibit scaling. Growth models give discrete sets of rules which determine how the surface evolves as particles are deposited. We were interested in the Das Sarma-Tamborenea (DT) model which was proposed to describe surface growth by molecular beam epitaxy. For many such models, it is possible to obtain stochastic PDEs which describe the discrete growth rules in the continuum limit. For the DT model, a significant discrepancy was observed between the critical exponents of the discrete model and those of the proposed continuum equation. This has been the motivation for our project.

First, we simulated the discrete model and elaborated on previous numerical estimations of the critical exponents. In sections 2.1 and 2.2, we introduce the growth rules of the DT model and the dynamic scaling it obeys. Then, we outline the computational methods used for simulations and data analysis in section 3. Results for the simulations of the discrete model are presented and discussed in section 4.1.

The method used to obtain a continuum equation is shown in detail in section 2.3. A brief discussion of step function regularization is presented in section 2.4. Following similar computational methods, numerical results for the continuum equation are discussed in section 4.2.

Our results show that numerical solutions of the continuum equation obtained following a systematic method converges onto the discrete DT model under correct step function regularization. We made estimations for the critical exponents for the DT model in agreement with previous results. Due to time constraints, solutions of the continuum equation provided less reliable data for exponent analysis. The results may be improved significantly by simulations of larger lattices with more repetitions.

Declaration of work undertaken

I have undertaken the computational simulation and theory aspects of this project. This includes coding the simulation for the discrete DT model, going over previous literature on obtaining continuum equations for various growth models, numerically integrating the stochastic PDE, and finally, running the simulations through the HPC cluster to obtain data.

Abstract

The Das Sarma and Tamborenea growth model was simulated in 1+1 dimensions for lattice sizes $L \leq 1024$, without employing noise reduction techniques. Through an analysis of finite-size effects, the roughness exponent was estimated to be $\alpha \approx 1.07$. The growth exponent was found to be $\beta \approx 0.366$ from shorter simulations of larger lattices and the dynamical exponent was estimated to be $z \approx 3.3$. The continuum description of the DT model following the method proposed by *Vvedensky et al.* [1] was also analysed. The Langevin equation describing the model was numerically integrated for lattice sizes $L \leq 128$. With appropriate regularization of the step function, it was shown that the solutions of the Langevin equation converge to the simulations of the discrete model as the integration step is lowered. Finally, similar analysis of the critical exponents yielded the estimates $\alpha \approx 1.25$, $\beta \approx 0.369$, $z \approx 3.5$.

1 Introduction

Surface growth is one of the simplest examples of dynamical non-equilibrium processes with broad physical applications including wetting, crystal growth, coating and vapour deposition [2, 3]. In such processes, an interface between two media grows as parts are deposited onto it, and evolves in time with some structure characterized by fluctuations. It has been proposed that in most surface growth processes, the surface structure is self-similar [4]. As an immediate consequence of self-similarity, surface fluctuations exhibit dynamic scaling governed by critical exponents α, β and z which define universality classes.

We are interested in crystal growth, where the particles that constitute the surface are located at fixed lattice sites. This allows the surface configuration to be specified by the height of each site. For example, for a one dimensional lattice of length L, the surface configuration is

$$\mathbf{H} = \{h_1, h_2, \ldots, h_L\}, \tag{1}$$

where h_i is the height of the ith lattice site. In d dimensions, the surface configuration $\mathbf{H}$ would contain L^d entries.

The deposited particles interact with the surface. These interactions are described by *growth models*, which assign a set of rules for deposition and diffusion of particles onto the surface. One of the simplest examples of a growth model is the random deposition (RD) model, where the particles simply stick to the lattice sites they were incident at [5]. A simple modification to the RD model is to include surface diffusion, where the particles diffuse to the neighbouring site with the smallest height. This would yield the Edwards-Wilkinson (EW) model [6]. We are interested in the Das Sarma-Tamboranea (DT) model, which describes growth by molecular beam epitaxy (MBE).

MBE is a process developed to grow films of semiconducting materials. Beams of atoms or molecules are incident on the surface of the material in vacuum. The vacuum environment, coupled with a low deposition rate ensures epitaxial growth, meaning the crystal structure of the material is preserved [7]. We will not be concerned with the physics of MBE as it is contained in the model we consider. Physical motivations of the growth rules of the DT model are discussed in section 2.1.

There has been a significant theoretical effort to express discrete deposition and diffusion rules provided by growth models in the continuum limit by a stochastic differential equation [8]. This can be done with phenomenological [9] or systematic [1] approaches. As a result, Langevin equations with solutions that exhibit the same scaling as the original models are obtained. It has been proposed [9, 10] that the DT model is described by the Villain–Lai–Das Sarma (VLDS) equation:

$$\frac{\partial h}{\partial t} = \nu_4 \nabla^4 h + \lambda_{22} \nabla^2 (\nabla h)^2 + \eta(\vec{x}, t), \tag{2}$$

3

where the surface configuration $\mathbf{H}$ is now the continuous function $h(\vec{x}, t)$, ν_4 and λ_{22} are constants and η is Gaussian white noise. In $d = 1$, this equation yields the critical exponents $\alpha = 1, \beta = \frac{1}{3}$ and $z = 3$.

The DT model has attracted theoretical interest due to a significant discrepancy between the critical exponents predicted by the VLDS equation and those calculated from simulations of the discrete model. This discrepancy has been the motivation for our project. Our aim is to first simulate the discrete model and elaborate further on the previous estimations of the critical exponents. Then, we take a systematic approach to obtaining a Langevin equation, which is not necessarily equivalent to the VLDS equation, and numerically integrate it to see whether the continuum description agrees with the discrete model.

2 Theory

2.1 The DT model

The DT model was proposed to "bridge the gap" between two types of growth models: kinetic growth and MBE growth [11].

In kinetic growth models, interactions between the deposited particles and the surface have no characteristic time scale. Any diffusion or relaxation of particles occur instantaneously. Furthermore, it follows from the lack of a time scale that atoms are allowed to relax only once, after which they are fully incorporated into the surface. Examples of kinetic growth include random deposition, ballistic deposition, Edwards-Wilkinson and Wolf-Villain models [6, 11, 12]. It was found that a lot of kinetic growth models belong to the KPZ universality class [13, 14, 15].

In MBE growth, each particle hops between lattice sites with some hopping rate. The rate increases with temperature and decreases with the number of nearest neighbour bonds the hopping atom has at its initial lattice site. This makes the particles "prefer" sites with more nearest neighbour bonds. In this context, a bond is formed whenever two particles are adjacent. MBE growth differs from kinetic growth since there is a characteristic time scale defined by the hopping rate and belongs to its own universality class [11].

The DT model incorporates the diffusion in MBE growth without introducing a hopping rate. As sites with more nearest neighbour bonds are preferred, deposited particles in the DT model relax to the nearest *kink site* up to the nearest neighbours of the deposition site. In 1D, a site i is a kink site if $h_{i+1} > h_i$ or $h_{i-1} > h_i$. Particles are only allowed to diffuse once, and diffusion happens instantaneously. This makes the DT model belong to kinetic growth.
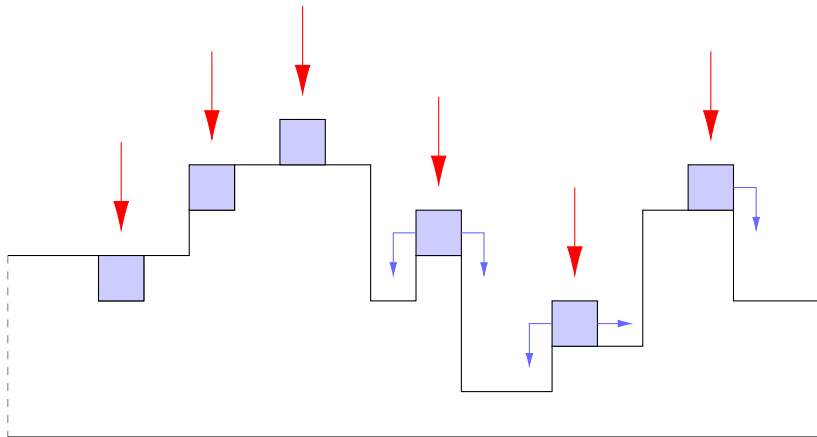
Figure 1: The growth rules for the DT model. Red arrows indicate the columns the particles are incident at. Blue arrows show where the particles diffuse.

The growth rules of the DT model are as follows: A site is chosen at random. If it is a kink site, the particle immediately sticks onto the chosen site. Otherwise, the particles relaxes to a nearest neighbour kink site. If both nearest neighbours are kink sites, one is chosen at random with equal probability. Finally, if neither nearest neighbours are kink sites, the particle sticks onto the initial site. These rules are summarised in Figure 1.

The Wolf-Villain (WV) model, proposed after the DT model, also attempts to describe MBE growth without incorporating continuous diffusion [12]. Again, kink sites are preferred due to the same physical motivation. However, in the WV model, the particles relax such that the coordination number is maximised, meaning not all kink sites are treated equally. Although the two models are very similar, the WV model was shown to belong to the Edwards-Wilkinson universality class [16].

2.2 Dynamic scaling

As the surface evolves in time, it does so with a certain structure. This is characterized by the fluctuations about the mean height of the surface. A measure of these fluctuations is the "surface width", defined for a surface of length L in d dimensions as

$$W(L,t) = \left[\left\langle \frac{1}{L^d} \sum_i \left(h_i - \bar{h} \right)^2 \right\rangle \right]^{1/2}, \tag{3}$$

where $\langle \cdot \rangle$ denotes an average over realizations, the index i runs over all lattice sites and $\bar{h}$ is the mean height. Due to a lack of a characteristic length or time scale, the width is expected to scale as a power law in time [3]:

$$W(L,t) \propto t^\beta, \tag{4}$$

where β is referred to as the "growth exponent" and describes how the correlations in the direction of growth increase with time.

For a finite surface of size L, the length over which fluctuations are correlated along the lattice can only grow up to L. If the system is evolved long enough, the correlations must saturate at L. Again, due to scale invariance, this finite-size effect is expected to give a scaling relation of the form [3]:

$$W(L, t \to \infty) \propto L^\alpha, \tag{5}$$

where α is called the "roughness exponent".

Relations (4) and (5) can be combined into a single scaling relation:

$$W(L,t) = L^\alpha f\left(t L^{-\alpha/\beta} \right), \quad \text{where} \quad f(u) = \begin{cases} u^\beta & u \ll 1, \\ \text{constant} & u \gg 1. \end{cases} \tag{6}$$

This dynamic scaling yields a characteristic "correlation time" $\tau \sim L^{\alpha/\beta}$, where the width saturates for $t \gg \tau$. This motivates the definition of the "dynamic scaling exponent" $z \equiv \alpha/\beta$.

The three exponents α, β and z, two of which are independent, define the universality class for any surface growth model. Finally, we note that the scaling relation (6) can be expressed independent of L under the rescaling of t and W as follows:

$$t \longmapsto t' = tL^{-z}, \quad W \longmapsto W' = WL^{-\alpha} \implies W'(L,t') = f(t'). \tag{7}$$

This rescaling will be used later on to obtain data collapse plots.

2.3 The Langevin equation

In this section, we present the systematic method proposed by *Vvedensky et al.* [1] to obtain a Langevin equation given the growth rules of a system. This is then applied to the DT model.

From equation (1), recall that the configuration of the surface is specified by $\mathbf{H}$. Let $P(\mathbf{H}, t)$ be the probability that the surface has configuration $\mathbf{H}$ at time t. The evolution of $P(\mathbf{H}, t)$ is given by the master equation [17]

$$\frac{\partial P(\mathbf{H}, t)}{\partial t} = \sum_{\mathbf{H}'} W(\mathbf{H}'; \mathbf{H}) P(\mathbf{H}', t) - \sum_{\mathbf{H}'} W(\mathbf{H}; \mathbf{H}') P(\mathbf{H}, t), \tag{8}$$

where $W(\mathbf{H}; \mathbf{H}')$ is the *transition rate* from configuration $\mathbf{H}$ to $\mathbf{H}'$ and the sums run over all possible configurations $\mathbf{H}'$.

In the limit of large system size, it has been shown by a limit theorem of *Kurtz* [18, 19, 20] that the master equation reduces to the Fokker-Planck equation:

$$\frac{\partial P(\mathbf{H}, t)}{\partial t} = -\sum_i \frac{\partial}{\partial h_i} \Big[K_i^{(1)}(\mathbf{H}) P(\mathbf{H}, t) \Big] + \frac{1}{2} \sum_{ij} \frac{\partial^2}{\partial h_i \partial h_j} \Big[K_{ij}^{(2)}(\mathbf{H}) P(\mathbf{H}, t) \Big], \tag{9}$$

where $K_i^{(1)}(\mathbf{H})$ and $K_{ij}^{(2)}(\mathbf{H})$ are the first and second transition moments of the transition rate $W(\mathbf{H}; \mathbf{H}')$, defined by

$$K_i^{(1)}(\mathbf{H}) = \sum_{\mathbf{H}'} (h_i' - h_i) W(\mathbf{H}; \mathbf{H}'), \tag{10}$$

$$K_{ij}^{(2)}(\mathbf{H}) = \sum_{\mathbf{H}'} (h_i' - h_i)(h_j' - h_j) W(\mathbf{H}; \mathbf{H}'). \tag{11}$$

The Fokker-Planck equation (9) is equivalent to the following Langevin equation in the Itô convention for stochastic calculus [21]:

$$\frac{\mathrm{d}h_i}{\mathrm{d}t} = K_i^{(1)}(\mathbf{H}) + \eta_i(t), \tag{12}$$

where the noise η_i has mean and variance

$$\langle \eta_i(t) \rangle = 0 \tag{13}$$

$$\langle \eta_i(t) \eta_j(t') \rangle = \delta(t - t') K_{ij}^{(2)}(\mathbf{H}). \tag{14}$$

The transition rate $W(\mathbf{H}; \mathbf{H}')$ and the associated moments $K_i^{(1)}$ and $K_{ij}^{(2)}$ are determined from the growth rules of the model. First, we let the lattice constant in the direction of growth be a, so if a particle sticks onto site i, $h_i \to h_i + a$. Also, we define the average deposition time for a monolayer (L particles) to be τ_0. In the DT model in one dimension, a particle can do one of three things: stick onto the incident site, diffuse left or right. We separate these three cases and write the transition rate as

$$W(\mathbf{H}; \mathbf{H}') = \frac{a}{\tau_0} \sum_k \Bigg[w_k^{(1)} \delta(h_k', h_k + a) \prod_{j \neq k} \delta(h_j', h_j) + w_k^{(2)} \delta(h_{k-1}', h_{k-1} + a) \prod_{j \neq k-1} \delta(h_j', h_j)$$

$$+ w_k^{(3)} \delta(h_{k+1}', h_{k+1} + a) \prod_{j \neq k+1} \delta(h_j', h_j) \Bigg], \tag{15}$$

where the first term accounts for a particle deposited at site k to stick at the deposited site, the second term for it to diffuse to $k-1$ and the third to diffuse to $k+1$. Each of the $w_k^{(1,2,3)}$ gives the probability to stick at the deposited site, diffuse left and right given a surface configuration **H**. To mathematically formulate the growth rules, the following definitions are used:

$$\theta(x) = \begin{cases} 1 & x \geq 0 \\ 0 & x < 0 \end{cases}, \quad \text{and} \quad \delta(x,y) = \begin{cases} 1 & x = y \\ 0 & x \neq y \end{cases}. \tag{16}$$

For example, a transition which would happen if $h_i > h_j$ would have a transition probability $(1 - \theta(h_j - h_i))$. The transition probabilities $w_k^{(1,2,3)}$ are therefore written considering every possible local surface configuration. For instance, consider $w_k^{(1)}$, which is the probability for a particle deposited at site k to stick at site k. Every possible surface configuration which will result in this can be listed as follows:

1. Site k is a kink $\implies h_{k+1} > h_k$ or $h_{k-1} > h_k$.

   (a) $h_{k+1} > h_k$ and $h_{k-1} > h_k \iff (1 - \theta(h_k - h_{k+1}))(1 - \theta(h_k - h_{k-1}))$.
   (b) $h_{k+1} > h_k$ and $h_{k-1} \leq h_k \iff (1 - \theta(h_k - h_{k+1}))\theta(h_k - h_{k-1})$.
   (c) $h_{k+1} \leq h_k$ and $h_{k-1} > h_k \iff \theta(h_k - h_{k+1})(1 - \theta(h_k - h_{k-1}))$.

2. Site k is not a kink $\implies$ sites $k \pm 1$ cannot be kinks.

   (d) $h_k = h_{k+1} = h_{k-1}$ and $h_{k-2} \leq h_{k-1}$ and $h_{k+2} \leq h_{k+1}$

   $$\iff \delta(h_k, h_{k+1})\delta(h_k, h_{k-1})\theta(h_{k+1} - h_{k+2})\theta(h_{k-1} - h_{k-2}).$$

Since all of these cases are mutually exclusive, the transition probability $w_k^{(1)}$ is the sum

$$\begin{aligned} w_k^{(1)} =& (1 - \theta(h_k - h_{k+1}))(1 - \theta(h_k - h_{k-1})) \\ &+ (1 - \theta(h_k - h_{k+1}))\theta(h_k - h_{k-1}) \\ &+ \theta(h_k - h_{k+1})(1 - \theta(h_k - h_{k-1})) \\ &+ \delta(h_k, h_{k+1})\delta(h_k, h_{k-1})\theta(h_{k+1} - h_{k+2})\theta(h_{k-1} - h_{k-2}). \end{aligned} \tag{17}$$

The transition probabilities $w_k^{(2,3)}$ are written following the same method. The identity

$$w_k^{(1)} + w_k^{(2)} + w_k^{(3)} = 1 \tag{18}$$

holds as expected. Substituting expression (15) into equations (10) and (11) yields

$$K_i^{(1)}(\mathbf{H}) = \frac{a}{\tau_0}\left[w_i^{(1)} + w_{i+1}^{(2)} + w_{i-1}^{(3)}\right], \tag{19}$$

$$K_{ij}^{(2)}(\mathbf{H}) = aK_i^{(1)}\delta_{ij}. \tag{20}$$

The continuum limit corresponds to letting $a \to 0$ and $\tau_0 \to 0$ such that $a/\tau_0 \to$ constant. Then, the surface configuration becomes a continuous function $\mathbf{H}(t) \to h(\vec{x}, t)$. After an analytic expansion of the transition rates $w^{(1,2,3)}$ is performed, the leading terms in a was shown to reproduce the VLDS equation [10]. However, we won't follow this approach and instead discretise equation (12) directly.

The Langevin equation is discretised in the Itô interpretation as follows [8, 22]:

$$h_i(t + \Delta t) = h_i(t) + \Delta t K_i^{(1)}(\mathbf{H}) + \left[\Delta t K_i^{(1)}(\mathbf{H})\right]^{1/2}\xi_i(t), \tag{21}$$

where the noise $\xi_i(t)$ obeys

$$\langle \xi_i(t) \rangle = 0, \quad \langle \xi_i(t)\xi_j(t') \rangle = \delta_{ij}\delta(t - t').$$

7

2.4 Step function regularization

Note that the Langevin equation (12) is expressed in terms of the transition probabilities $w^{(1,2,3)}$, each of which is expressed in terms of the step and delta functions defined by (16). In the discrete model, $x = h_i - h_j$ takes on only integer values. However, in the continuum limit the height differences can take any real value. We must choose an appropriate continuation of the step function in the range $x \in [-1, 0]$ such that the growth rules of the model are preserved. A simple regularization that was shown to work is [8]:

$$\theta(x; a) = \begin{cases} 1 & x \geq 0, \\ (x+a)/a & -a < x < 0, \\ 0 & x \leq -a, \end{cases} \tag{22}$$

where $a \in (0, 1]$. The parameter a is chosen such that the growth rules of the model are preserved for non-integer height differences.
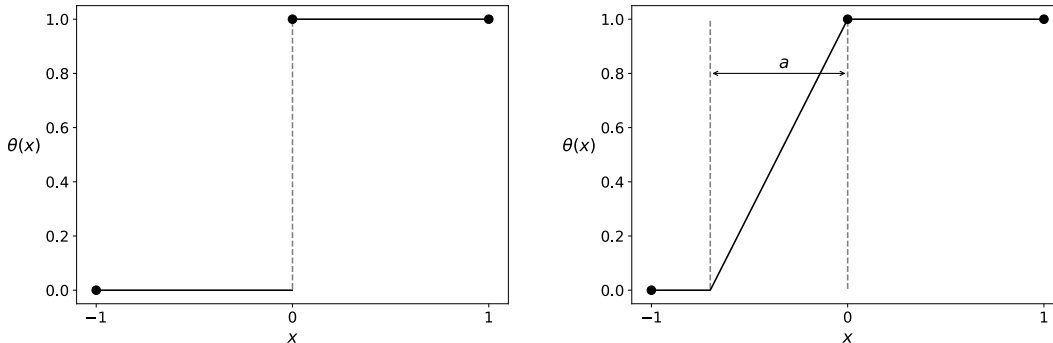
Figure 2: Step function with (left) no regularization and (right) regularization with some $a < 1$.

It was shown [8] that for the Edwards-Wilkinson model $a = 0$ and for the Wolf-Villain model $a = 1$. Due to the similarities between WV and DT models, we would expect the correct regularization for the DT model to be $a = 1$. Moreover, there is physical motivation to justify setting $a = 1$. When the height differences can take any real value, the probability of neighboring heights being equal becomes zero. This means the transition rules that depend on equal heights are never applied. As mentioned in section 2.1, the rules of the DT model are motivated by the MBE process where the number of bonds determine how energetically preferable a site is. Setting $a = 0$ would correspond to a sharp transition where an infinitesimal height difference becomes physically equivalent creating or breaking a bond. This can be avoided by applying the rules gradually, setting $a = 1$. This is also confirmed by data, shown in section 4.2.

3 Computational Methods

3.1 Methods for simulations

All simulations were coded in C++. For the discrete model, the deposition rules are checked and applied given the local surface configurations. Firstly, the surface is represented by an array of integers which we will refer to as the "surface array". Each position in the array corresponds to a lattice site, with the associated integer value corresponding to the number of particles deposited to that site. For a surface of length L, an array of size L is created. Periodic boundary conditions are applied.

The surface array is initialized flat, with zero height at every site. Particles are deposited as follows: First, a random site is chosen. A check is performed to determine whether the chosen site, or the two nearest neighbours are kink sites or not. Then, the particle is placed on the surface array according to the growth rules.

The Mersenne twister engine (std::mt19937) was used to generate random numbers. As particles were deposited, the width of the surface was calculated on evenly spaced time intervals on a logarithmic scale. Typically, consecutive measurements were taken at times $t_{n+1} = \lambda t_n$ where $\lambda = 1.01$. In all simulations, a time unit corresponds to the deposition of a monolayer. For a lattice of size L, a time unit would be the deposition of L particles.

Due to the randomness in the growth process, every simulation was repeated and the width averaged over multiple realizations. As the time unit depends on L, the process is "self-averaging". For larger lattices, fewer realizations are sufficient to obtain smoother data.

Since the correlation time τ scales with a power law in L (see section 2.2), simulation times increase very rapidly with increasing L. Assuming that the total number of depositions in a simulation is proportional to the computational time, simulations ran until time τ have time complexity $\mathcal{O}(L^{1+z})$, where typically $z \sim 3$. This presented two problems for the simulation: overflows in the surface array entries and long computing times.

To prevent overflows, the surface array was periodically "reduced". This means the minimum height of the surface array was subtracted from each entry. The simulations were coded in C++ for higher computing performance. Finally, both discrete and continuum simulations were run in the High Performance Computing (HPC) cluster at Imperial College.

Numerical integration of the Langevin equation is done by evolving equation (21) by Euler's method. The first moment of the transition rate $K_i^{(1)}$ is expressed explicitly in terms of $w^{(1,2,3)}$. Armadillo library [23] is used for linear algebra. The same method for calculating the width averaged over many realizations is implemented.

3.2 Methods for exponent analysis

Here, we outline the methods we used to extract the critical exponents α, β and z.

Exponents α and β are related to the behaviour of the width in the saturation and growth regimes respectively. Therefore, we needed a systematic way of identifying the two regimes. By the scaling relation (6), the width is linear in time on a logarithmic scale in both regimes with gradient β in the growth, and zero gradient in the saturation regime. This allowed us to identify the two regimes by considering the goodness of linear fits.

For the saturation regime, we considered linear fits starting from some point $t_0 = 10^3$, ending at the last data point. Then, we incrementally moved the starting point t_0 up to the end, each time calculating the R^2-coefficient of the corresponding linear fit. We define the saturation regime to begin at the time corresponding to the first local minimum of the R^2 value. The global minimum was unreliable due to the noise in the saturation regime.

Similarly, for the growth regime, we considered linear fits from $t_0 = 10^3$ up to the end. Then, we incrementally moved the end point down to t_0, calculating the R^2 coefficient. As the growth regime had much less noise, we defined the end of the growth regime to be the global minimum of the R^2 value. An illustration of the results of this method is shown on Figure 3. A different method using the R^2 coefficient was previously proposed by *Aarão Reis et al.* [24].

The roughness exponent α is related to the saturation width. One way to extract α is to plot the saturation width against the lattice size L. Then, α would correspond to the gradient on a logarithmic scale. However, just calculating the gradient would result in "averaging out" any relationship between α and L due to finite size effects, which in turn would yield an unreliable asymptotic value for α as $L \to \infty$. Instead, we used the following definition for the roughness exponent [24]:

$$\alpha_L = \frac{\log(W_{\text{sat}}(L)) - \log(W_{\text{sat}}(L/2))}{\log 2}, \tag{23}$$
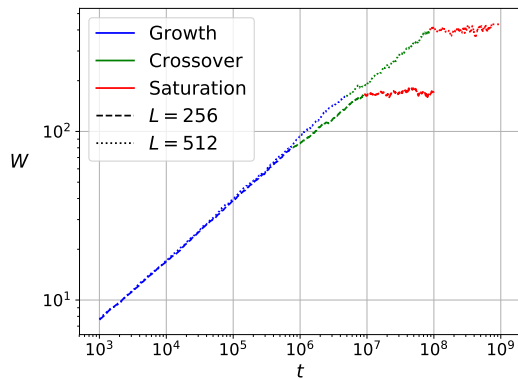
Figure 3: Growth, crossover and saturation regimes, shown in blue, green and red, of discrete simulations for lattice sizes $L = 256, 512$ shown by dashed and dotted curves.

where $W_{\text{sat}}(L)$ is the saturation with for lattice size L. As $L \to \infty$, α_L is expected to converge to an asymptotic value. Looking at how α_L varies with L, the asymptotic value for α is estimated.

The growth exponent β was estimated from the gradient of the linear fit in the growth region. Since the saturation width does not play a role, we ran shorter simulations for much larger lattice sizes, up to $L = 16384$, for times until $t = 10^5$. Then, β was estimated from the linear fit in the time range $t \in [10^3, 10^5]$.

Finally, the dynamical exponent z was obtained from the saturation time τ. On a logarithmic scale, it corresponds to the gradient of τ with respect to L due to the relation $\tau \propto L^z$. A similar definition to the roughness exponent may be used, so that

$$z_L = \frac{\log(\tau(L)) - \log(\tau(L/2))}{\log 2}.$$

But finite size effects did not display any significant correlation between τ_L and L and so this method was not implemented.

4 Results

4.1 Discrete model

First, we simulated the DT model according to the discrete growth rules. The simulations shown on Figure 4 were run until the widths saturated for lattice sizes up to $L = 512$. The scaling form given by equation (6) is clearly observed. As the lattice size was increased, due to the rapidly increasing computation times, the number of realizations was decreased. This accounts for the increase in noise for the larger lattice sizes, visible most clearly in the saturation region.

The roughness exponent is estimated by a method proposed in [24]. By equation (23), α_L is calculated. Then, a correction term $L^{-\Delta}$ to equation (5) is considered of the form

$$\alpha_L = \alpha + L^{-2\Delta} + L^{-\Delta},$$

where α is the asymptotic value of α_L as $L \to \infty$. A second-degree polynomial is fitted to the data on a $\alpha_L \times L^{-\Delta}$ plot. The correction Δ is chosen such that the fit covariance is minimised. This turned out to be $\Delta = 0.3868 \pm 0.0001$. The result is shown on Figure 5a, alongside a plot of $\alpha_L \times L$ on Figure 5b which shows how the roughness exponent changes due to finite-size effects. The asymptotic value of α is estimated to be $\alpha = 1.07 \pm 0.02$, where the errors are obtained from the covariance of the fit.

10
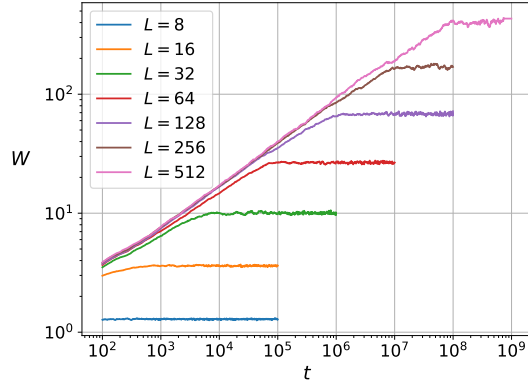
Figure 4: Time evolution of the surface width for different lattice sizes $L \leq 512$ in the discrete DT model.

| (a) | (b) |
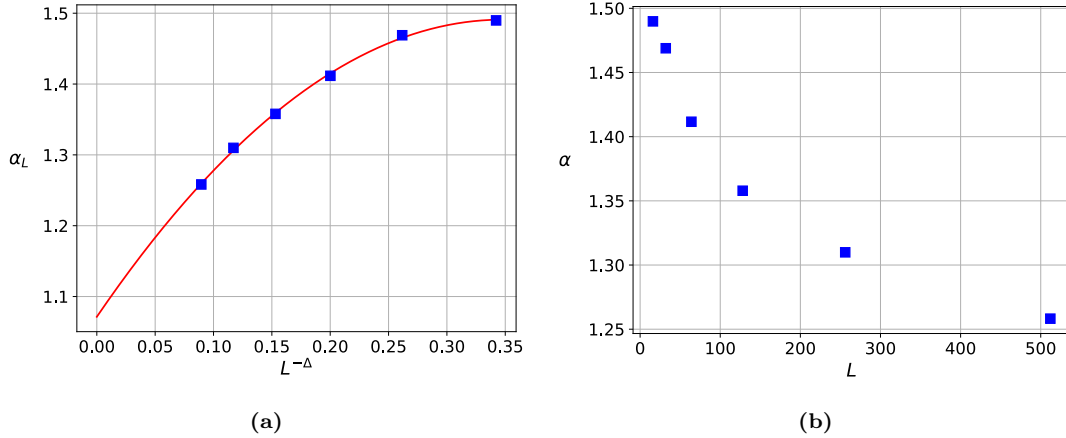
Figure 5: Roughness exponent α_L as a function of (a) the correction $L^{-\Delta}$ with a second degree polynomial fit, and (b) lattice size L.

For the growth exponent, the results of the larger simulations are summarised on Table 1, obtained by the method outlined in section 3.2. The errors are estimated from the covariance of the fit. Since there is no clear trend towards an asymptotic value, we conclude that the variations in β are due to the randomness of the growth process and the limited number of realizations. The average value of β is $\overline{\beta} = 0.3663 \pm 0.0002$.

Lattice Size	β
2048	0.3645 ± 10^{-4}
4096	0.3668 ± 10^{-4}
8192	$0.36739 \pm 9 \times 10^{-5}$
16384	$0.36654 \pm 9 \times 10^{-5}$

Table 1: β values obtained from linear fits in the time range $t \in [10^3, 10^5]$ with 250 realizations.

The dynamical exponent z is estimated from the saturation time τ. A plot of $\tau \times L$ is shown on Figure 6, with a fit that is linear on logarithmic scale. The gradient of the fit gives the estimate $z = 3.33 \pm 0.07$, where the error is again obtained from the covariance of fit.

11
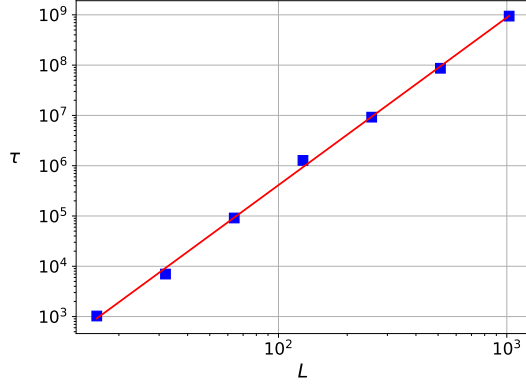
Figure 6: The saturation time τ against lattice size L, for lattice sizes up to $L = 1024$. The linear fit is shown in red.

The estimate obtained for z is not consistent with α and β, considering the relationship $z = \alpha/\beta$. However, the value is similar to that obtained by *Costa, Euzebio and Aarao Reis* [24]. The discrepancy may be due to different scaling behaviour at larger lattice sizes.

(a)

(b)
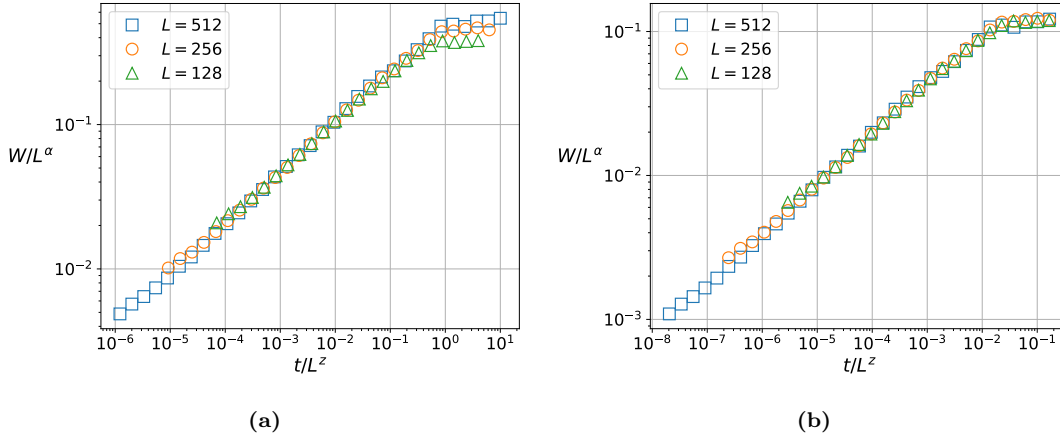
Figure 7: Data collapse plot for exponents (a) $\beta = 0.3663$, $\alpha = 1.07$, and (b) $\alpha = 1.31$. The dynamical exponent is $z = \alpha/\beta$.

Finally, using the estimates for the exponents, we may rescale the time and width axes according to equation (7) to obtain a data collapse plot. This is shown on Figure 7 for two different values for α. On Figure 7a, the asymptotic value for $\alpha = 1.07$ is used. It is clear that the saturation widths for the lattice sizes shown do not overlap. This is due to finite-size effects, and shows that the lattice sizes are not large enough to obey the asymptotic exponents. On Figure 7b, $\alpha_L = 1.31$ is used. This is the roughness exponent calculated by equation (23) for $L = 256$. The overlap in the saturation regime is much better for this choice of α as expected. In both cases, the growth regime shows good overlap. This shows that the asymptotic scaling behaviour in the growth region is very similar to the scaling seen in the simulations for finite size lattices.

12

4.2 Continuum equation

All results presented in this section follow from numerical integration of equation (21) with various time steps. First, the convergence to the discrete model for different time steps and regularizations is shown. This is followed by a similar analysis of the exponents α, β and z.

In section 2.4, we emphasized the importance of choosing the correct regularization for the step function. Here, we present the quantitative difference between different choices of regularization. On Figure 8a, the results of integrating the Langevin equation with two different regularizations are shown for $L = 16$ and $\Delta t = 0.001$. The regularization given by equation (22) is implemented with $a = 1.0$ and $a = 0.01$. As expected, the continuum results converge on to the discrete model when $a = 1.0$.

It is expected that as the numerical integration is carried out with smaller time steps, in the limit $\Delta t \to 0$ the continuum results converge to the simulations of the discrete model. Figure 8b shows the results of integrating with two different time steps for $L = 128$ and $a = 1.0$. As the time step is lowered, a better overlap between the continuum results and the discrete simulation is observed. Although the overlap in the saturation regime is significant for $\Delta t = 0.1$, the growth regime still shows discrepancies. This suggests a slower convergence between the continuous and discrete simulations in the growth regime.
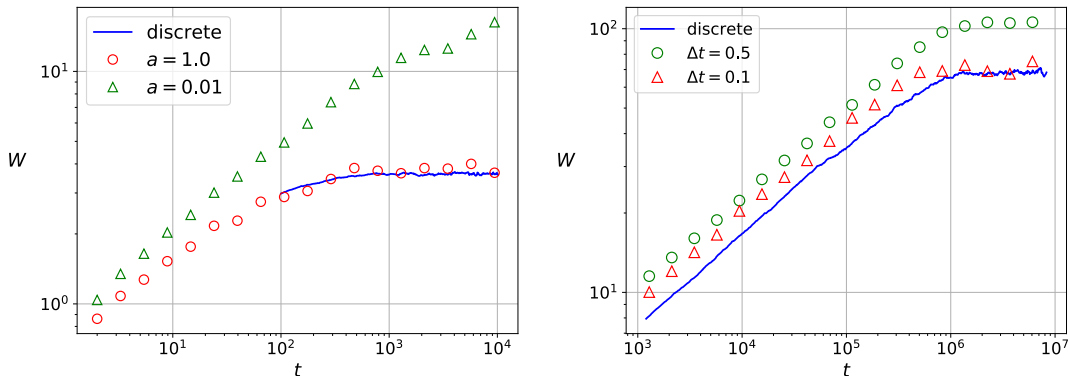
(a) Different regularizations a at fixed time step $\Delta t = 0.001$ and lattice size $L = 16$.

(b) Different time steps Δt at fixed regularization $a = 1.0$ and lattice size $L = 128$.

Figure 8: Convergence of the numerical integration of the Langevin equation for different step function regularizations and time steps.

The results for numerically integrating the Langevin equation starting from $L = 8$ up to $L = 128$ with time step $\Delta t = 0.1$ and regularization $a = 1.0$ is shown on Figure 9. We can identify the growth and saturation regimes clearly and the results obey the general scaling relation given by equation (6).

Due to the much greater computational cost of integrating the Langevin equation compared to the discrete model, the data for the continuum simulations is limited. This means the analysis of the critical exponents will be less reliable compared to the discrete simulations.

The roughness exponent is estimated following a similar method used for the discrete model. Instead of a second degree polynomial, a linear fit is used with correction exponent $\Delta = 0.45865 \pm 0.0001$, so that

$$\alpha_L = \alpha + L^{-\Delta}.$$

This method was previously used to estimate KPZ exponents from the ballistic deposition model [25]. The results are shown on Figure 10. The asymptotic value for α_L is obtained by extrapolating the linear fit shown on Figure 10b. This gives $\alpha = 1.25 \pm 0.01$. This is significantly different from the roughness exponent obtained from the discrete simulations.

13
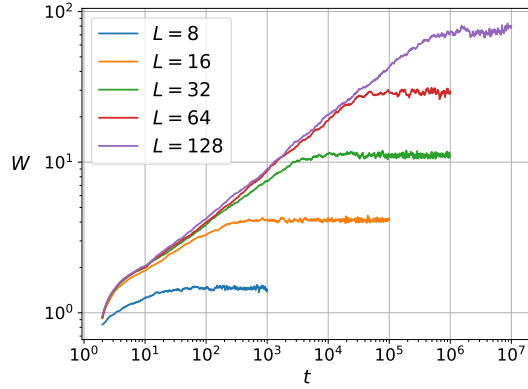
Figure 9: Results of numerically integrating the Langevin equation with time step $\Delta t = 0.1$ for lattice sizes $L \le 128$.

| (a) | (b) |
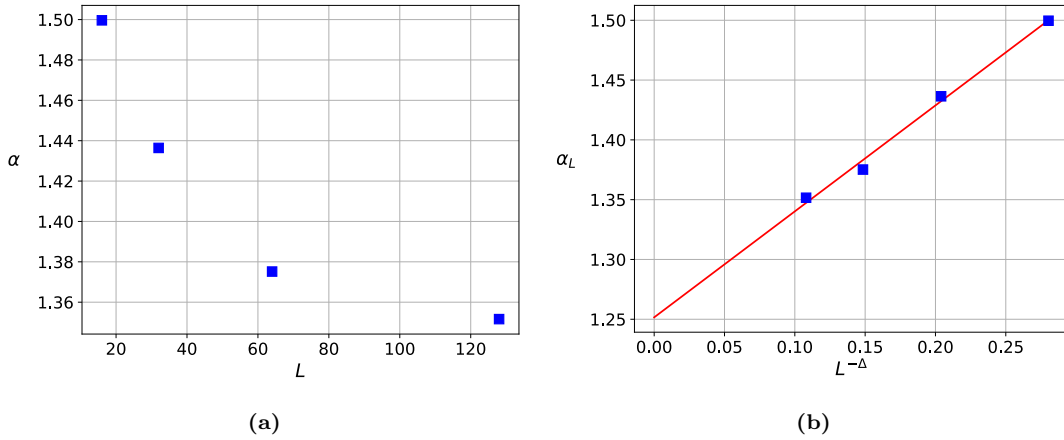
Figure 10: Roughness exponent α_L as a function of (a) L and (b) $L^{-\Delta}$ with a linear fit shown in red.

The growth exponent β is estimated in the same manner as before. Results of the larger simulations are shown on Table 2. Errors are obtained from the covariances of the linear fits. The average β is $\bar{\beta} = 0.3691 \pm 0.0006$. This is in closer agreement with the discrete model.

Lattice Size	β
512	0.3604 ± 0.0003
1024	0.3739 ± 0.0003
2048	0.3730 ± 0.0004

Table 2: β values obtained from linear fits in the time range $t \in [10^3, 10^4]$ with 100 realizations.

Finally, we follow the same method as before to obtain an estimate for the dynamical exponent z. A plot of $\tau \times L$ is shown, with an associated fit on Figure 11. The z value obtained from the gradient is $z = 3.5 \pm 0.2$. This result agrees with the simulations of the discrete model within uncertainty. We can estimate z by the relation α/β, which gives

$$z = \frac{\alpha}{\beta} = 3.39 \pm 0.03,$$

which is consistent with the estimate for z obtained from the saturation time.

14
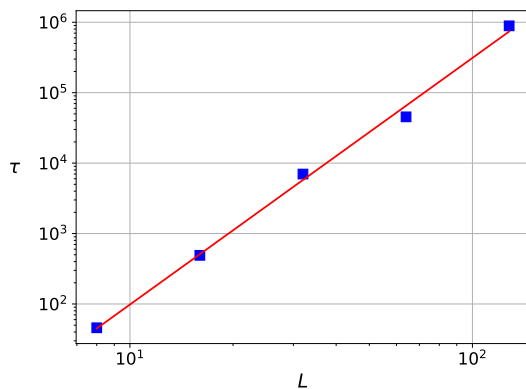
Figure 11: Saturation time τ against L, with a fit linear on a logarithmic scale.

Combining the estimates for α, β and z, we can again obtain a data collapse plot. For $\alpha = 1.25$ and $\beta = 0.3691$, this is shown on Figure 12. The overlap in both the growth and saturation regimes are good. This is not surprising as the asymptotic value estimated for α is much closer to α_L for $L = 128$. Compared to the discrete simulations, finite size effects are less prominent especially regarding the saturation width.
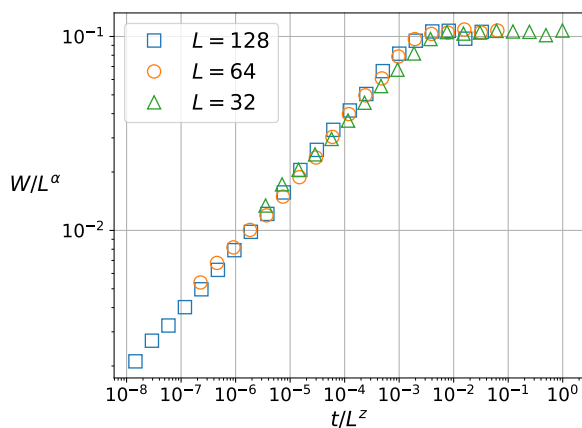
Figure 12: Data collapse of continuum simulations for $\alpha = 1.25$, $\beta = 0.3691$ and $z = \alpha/\beta$.

Differences between the critical exponents and their dependence on finite-size effects observed between the discrete and continuum simulations may be due to a number of different factors. Firstly, the data for the continuum simulations are much more limited in terms of the lattice sizes considered. Furthermore, the time step used for the continuum simulations may not be small enough to exhibit the same finite-size effects as the discrete DT model in the continuum limit.

5 Conclusion

We simulated the Das Sarma-Tamborenea (DT) model for MBE growth in one dimensional surfaces. Using the dynamical scaling of the surface width, we estimated asymptotic values for the critical exponents α, β and z. The roughness exponent was estimated to be $\alpha = 1.07 \pm 0.02$

by an analysis of finite-size effects, in agreement with previous results [24]. For the growth exponent, shorter simulations were carried out for much larger lattices. This yielded an average value of $\beta = 0.3663 \pm 0.0002$. Finally, the dynamical exponent was found to be $z = 3.33 \pm 0.07$, which was estimated using the saturation time. Our asymptotic estimates are not consistent with the relation $z = \alpha/\beta$, which suggests the presence of different scaling behaviour for larger lattice sizes. The discrepancies may be resolved by running simulations for larger lattices, which we were unable to do due to time constraints.

The description of the DT model in the continuum limit was also studied. We followed the method proposed by *Vvedensky et. al.* [1] to obtain a Langevin equation [10]. After applying an appropriate step function regularization, we numerically integrated the Langevin equation. This showed that, with the correct regularization, the solutions of the Langevin equation converge to the simulations of the DT model as the time step is lowered. Afterwards, a similar analysis of the critical exponents was carried out for the continuum simulations with time step $\Delta t = 0.1$. This yielded the values $\alpha = 1.25 \pm 0.01$, $\beta = 0.3691 \pm 0.0006$ and $z = 3.5 \pm 0.2$. The dynamical and growth exponents are close to the discrete model, however the roughness exponent shows significant discrepancy. These discrepancies can again be further studied by running simulations for larger lattice sizes with smaller time steps.

Compared with the predictions of the VLDS equation which suggest $\alpha = 1, \beta = \frac{1}{3}$ and $z = 3$, our results are significantly different. Only the estimate for the roughness exponent for the discrete model shows good agreement, whereas the growth and dynamical exponents differ significantly. This discrepancy persists for the simulations of the continuum model as well, which confirms that the DT model exhibits significantly different scaling for larger lattice sizes. The agreement between the numerical integration of the Langevin equation and the simulations of the discrete model shows the validity of the systematic method used to obtain the Langevin equation, and further suggests that equation (12) may reduce to the VLDS equation in the continuum limit of the lattice constant $a \to 0$. A more detailed analysis of taking this limit, including further analysis using renormalization group theory as well as running larger simulations of the discrete model would be appropriate extensions of the work presented here.

Acknowledgements

References

[1] D. D. Vvedensky, A. Zangwill, C. N. Luse, and M. R. Wilby, "Stochastic equations of motion for epitaxial growth," *Physical Review E*, 1993.

[2] M. Kardar, *Statistical Physics of Fields*. 2007.

[3] F. Family and T. Vicsek, *Dynamics of Fractal Surfaces*. 1991.

[4] R. P. Burn and B. B. Mandelbrot, "The Fractal Geometry of Nature," *The Mathematical Gazette*, 1984.

[5] F. Family, "Scaling of rough surfaces: Effects of surface diffusion," *Journal of Physics A: Mathematical and General*, 1986.

[6] S. Pal, D. P. Landau, and K. Binder, "Dynamical scaling of surface growth in simple lattice models," *Physical Review E - Statistical Physics, Plasmas, Fluids, and Related Interdisciplinary Topics*, 2003.

[7] J. R. Arthur, "Molecular beam epitaxy," *Surface Science*, 2002.

[8] A. L. Chua, C. A. Haselwandter, C. Baggio, and D. D. Vvedensky, "Langevin equations for fluctuating surfaces," *Physical Review E - Statistical, Nonlinear, and Soft Matter Physics*, 2005.

[9] Z. W. Lai and S. Das Sarma, "Kinetic growth with surface relaxation: Continuum versus atomistic models," *Physical Review Letters*, 1991.

[10] Z. F. Huang and B. L. Gu, "Growth equations for the Wolf-Villain and Das Sarma-Tamborenea models of molecular-beam epitaxy," *Physical Review E - Statistical Physics, Plasmas, Fluids, and Related Interdisciplinary Topics*, 1996.

[11] S. Das Sarma and P. Tamborenea, "A new universality class for kinetic growth: One-dimensional molecular-beam epitaxy," *Physical Review Letters*, 1991.

[12] J. Villain and D. E. Wolf, "Growth with surface diffusion," *EPL*, 1990.

[13] M. Kardar, G. Parisi, and Y. C. Zhang, "Dynamic scaling of growing interfaces," *Physical Review Letters*, 1986.

[14] E. Medina, T. Hwa, M. Kardar, and Y. C. Zhang, "Burgers equation with correlated noise: Renormalization-group analysis and applications to directed polymers and interface growth," *Physical Review A*, 1989.

[15] J. M. Kim and J. M. Kosterlitz, "Growth in a restricted solid-on-solid model," *Physical Review Letters*, 1989.

[16] D. D. Vvedensky, "Crossover and universality in the Wolf-Villain model," *Physical Review E - Statistical Physics, Plasmas, Fluids, and Related Interdisciplinary Topics*, 2003.

[17] V. N. G. Kampen, *Stochastic Processes in Physics and Chemistry*. 2007.

[18] T. G. Kurtz, "Strong approximation theorems for density dependent Markov chains," *Stochastic Processes and their Applications*, 1978.

[19] H. A. Kramers, "Brownian motion in a field of force and the diffusion model of chemical reactions," *Physica*, 1940.

[20] J. E. Moyal, "Stochastic Processes and Statistical Physics," *Journal of the Royal Statistical Society: Series B (Methodological)*, 1949.

[21] R. F. Fox and J. Keizer, "Amplification of intrinsic fluctuations by chaotic dynamics in physical systems," *Physical Review A*, 1991.

[22] J. L. Doob, "The Brownian Movement and Stochastic Equations," *The Annals of Mathematics*, 1942.

[23] C. Sanderson and R. Curtin, "Armadillo: a template-based C++ library for linear algebra," *The Journal of Open Source Software*, 2016.

[24] B. S. Costa, J. A. Euzébio, and F. D. Aarão Reis, "Finite-size effects on the growth models of Das Sarma and Tamborenea and Wolf and Villain," *Physica A: Statistical Mechanics and its Applications*, 2003.

[25] F. D. Aarão Reis, "Universality and corrections to scaling in the ballistic deposition model," *Physical Review E - Statistical Physics, Plasmas, Fluids, and Related Interdisciplinary Topics*, 2001.

The code used to obtain the data can be found in the Github repository:

https://github.com/emre-ozer/dt_model_simulations